Performance Analysis of Three-Phase Interleaved Buck-Boost Converter in Wind Energy Maximum Power Point Tracking

Muhammad Qasim Nawaz[*], Wei Jiang[**], Aimal Khan[***]

[*, **, ***] Department of Electrical Engineering and Automation, Yangzhou University, China
Email: qasimnawaz27@gmail.com [*]
[*]https://orcid.org/0009-0007-8892-4599

[**]Email: weijiang@yzu.edu.com
https://orcid.org/0009-0007-8042-4485

[***]Email: aimal.bsee@gmail.com
https://orcid.org/0009-0007-7841-99457

Abstract

This paper presents a performance analysis of a three-phase interleaved buck-boost converter integrated with a Maximum Power Point Tracking (MPPT) algorithm using the Perturb and Observe (P&O) method for an independent wind energy generation system. The P&O method effectively identifies and tracks the maximum power point (MPP) under varying wind conditions. The use of a three-phase interleaved converter improves the power conversion efficiency and reduces input current ripple while distributing thermal stress across multiple phases. Simulation results, conducted via MATLAB, demonstrate a significant increase in overall system efficiency, with power extraction efficiency improving by up to 20% compared to traditional single-phase converters. The converter also reduces current ripple by approximately 30%, enhancing stability during variable wind profiles. The system responds accurately to wind speed changes, ensuring optimal energy extraction across various operational conditions. This study provides practical insights into the design and application of advanced power converters and MPPT controllers in wind energy systems, offering a pathway toward improved energy management and reliability in wind energy conversion systems.

Keywords- Three-Phase Interleaved Buck-Boost Converter, Wind Energy Conversion Systems (WECS), Optimisation of Power Extraction, Wind Turbines.

I. INTRODUCTION

The upward growth in global wind energy capacity and graph, as seen in Figure 1, which achieved 906 GW and has gone up 9% for the last year itself emphasises the need to develop strategies towards the fullest development of wind energy systems. This upward trend indicates that more renewable energy sources will be utilised to satisfy the growing need for energy in the world [1]. Tracking the Maximum Power Point for Wind Energy Conversion Systems (MPPT) controls the power, adjusting the perturbation of the WECS, where perturbation is a “heal and poke” techniques. Among them, the P&O method is extensively utilised to monitor the MPP, or maximum power point, in varying wind condition which represents a critical issue for improving the efficiency and performance of wind turbine systems [2]. This is due to the simple fact that the system operates by changing the operating point of the wind turbine and observing the power output. In such methods, the MPP is approached, and the power output is optimised by taking note of the changes in that power output. Even though MATLAB is not part of the P&O MPPT algorithm, it provides commercial and T-permitting standard mass production. It allows for the quantitative analysis of different perturbation sizes and response times, which are of paramount importance in achieving the required efficiency, given some changing wind dynamics. Being able to run P&O MPPT MATLAB simulation makes it possible to evaluate how diverse cases of varying wind speed and turbulence would affect the performance of the system. This is important, as when properly done, it allows the algorithm to be optimised such that the potential of the wind energy system is not surpassed. The additional inclusion of a three phase interleaved buck-boost converter further augments this procedure by enhancing the efficiency of power conversion and rendering better management of output voltage and current [3]. The converter employs an interleaving technique in order to alleviate input current ripple voltage and balance thermals over several phases, which greatly enhances the performance of the entire system. It has been demonstrated in simulations that the combination of the P&O MPPT with an interleaved buck-boost converter with three phases significantly improves power extraction efficiency and increases energy, which is therefore taken from wind resources.

This research not only demonstrates the practical applications of the advanced MPPT algorithms and power conversion technologies in wind energy equipment but also prepares ground for the design and deployment of more dependable and effective renewable energy systems. As the world proceeds on the path of sustainable energy, the necessity of concepts like these gets ever higher [4]. These efforts support the development of future technologies relating to wind energy and assist in building structures that can withstand the energy demands of the world while minimising resource wastage. The P&O MPPT algorithm's application in the MATLAB environment for MPPT of wind energy systems is a good development in the enhancement of performance and reliability of renewable energy systems. [5]

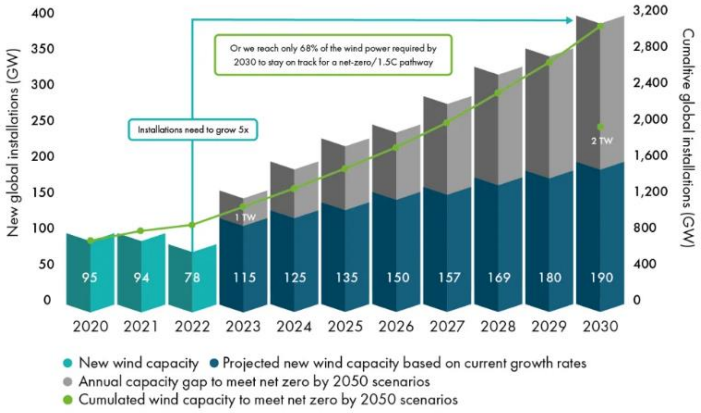

Figure 1: Total wind power capacity additions from 2020–2030 [1]

Figure 2 shows the power flow within a WECS, particularly focusing on interpreting the MPPT control of the interleaved buck-boost converter with three phases. The PMSG, or permanent magnet synchronous generator, is attached to the turbine. In this model of wind energy, the turbine is powered by wind energy, which, in this case, is V_{wind}. The rectifier is capable of converting electricity generated by the PMSG module from mechanical energy to electrical energy. A design which comprises of a three-phase interleaved buck-boost converter, a system that facilitate power transfer by changing the voltage and current levels to be appropriate, accept such the DC power [5]. This converter is fitted with an MPPT controller that is based on the Perturb and Observe (P&O) algorithm and modifies the system's operating point. Constantly in order to harvest as much wind energy as possible. The processed electricity is stored in a battery so as to provide different types of loads [6] [7]. The complete design is aimed at maximising the power output of the wind energy conversion arrangement system and the operating flexibility of the system under different wind conditions.

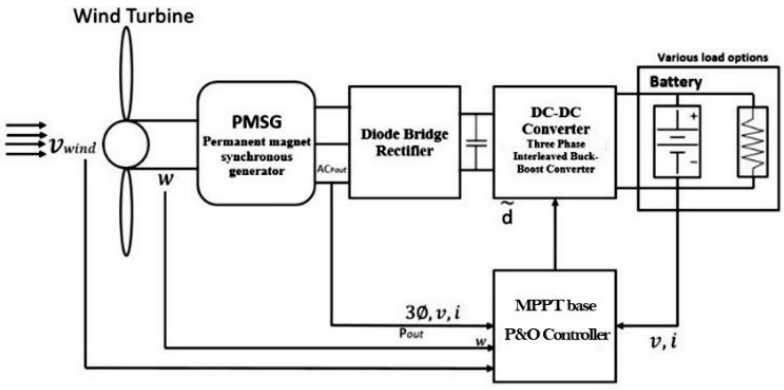

Figure 2: Schematic of the proposed multiphase WECS. [4]

Figure 3 depicts a structure of a buck-boost converter with three phases interleaved developed for Maximum Power Point Tracking (MPPT) functions in wind energy harvest systems. The basic construction of the system contains three interleaved phases as well as harnesses the switches and diodes to control the input voltage V_{in} using inductors L and resistors RL, whereby the inductor currents i_1, i_2, i_3, in are first filtered and combined at the output stage. This configuration helps decrease the amount of current ripple and improves the efficiency of the power conversion. Band pass filters composed of capacitors C and resistors RC have been employed in this circumstance to regulate the output voltage V_{out}. The total output current it is made available to the load, increasing the amount of energy obtainable from the wind. However, the converter uses the perturb and observe (P&O) technique for MPPT, which adjusts the operating point at every moment enhancing the power produced by the wind energy systems in operation [7] [8].

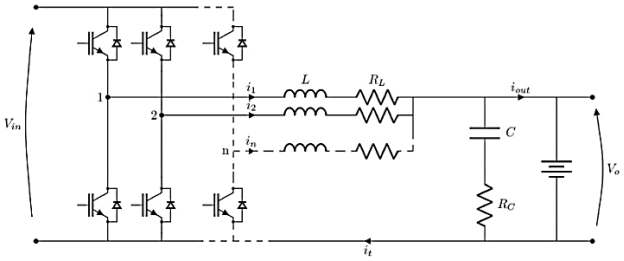

Figure 3: Multiphase Interleaved Buck-Boost Converter [4]

The three Phase Interleaved Buck-Boost Converter, which is also a Maximum Power Point Tracking MPPT, is used in Figure 4 to track the Maximum Power Point in a Wind Energy Conversion system using the Perturb and Observe (P&O) method. Setting the voltage V(0) starts the process. It formerly records the current $I_{(k)}$ and voltage $V_{(k)}$ instantaneously and computes Power $P_{(k)}=V_{(k)}I_{(k)}$. The algorithm uses the current and previous step values to calculate the power change (ΔP) and the voltage change (ΔV). If ΔP is positive, it implies more power is being generated, and in this case, the algorithm varies duty cycle D depending on whether ΔV is positive or negative. On the other hand, if ΔP is negative, the duty cycle is varied but in the reverse way [8]. The adjustments are repeated, resorting to the techniques until it is established that the system operates within the maximum power point, cutting down on the performance and efficiency losses of wind energy system by trying to optimise power out of the system via the converter.

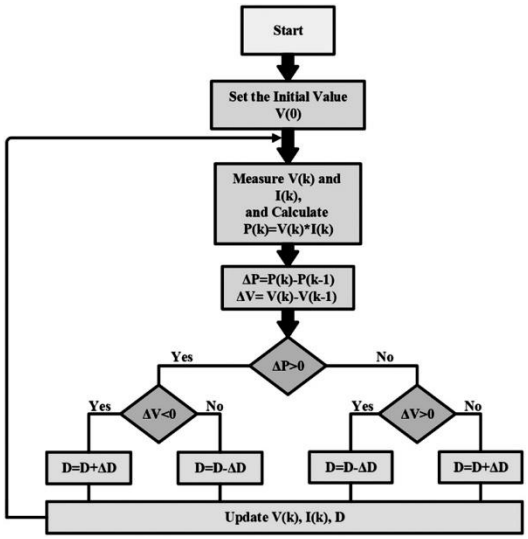

Figure 4: Perturbation and Observation MPPT flow chart [6]

II. LITERATURE REVIEW

The implementation of the TPIBBC technique in wind energy systems, especially in MPPT applications, has received notable focus considering the improved performance, boost in stability and enhancement in power quality. As explained by L. Pirashanthiyah et al. in 2024, the structure of TPIBBCs designed for use in photovoltaic systems can be transferred to wind energy systems by employing standard boost converters instead more of these parallel connections, enhancing efficiency and reliability (Pirashanthiyah et al., 2024) [9]. By this method of interleaving converters, i.e. operating a number of converters in parallel results in less current ripple and reduced heat thus leading to a much better efficiency of the total converter (Kiran Kumar et al., 2021) [9, 10]. Such techniques are very useful for wind energy systems where the input power is always varying. Therefore, in order to extract the maximum amount of energy from wind turbines, MPPT techniques such as the use of Incremental Conductance (INC) and Perturb and Observe (P&O) methods are essential. The TPIBBC has a fast dynamic response, which helps to execute these algorithms satisfactorily in a manner that adjustment in the duty cycle follows for MPP tracking (Krishnaram et al., 2024) [11]. Bastien utilised the P&O algorithm where the operating point is varied and the level of power produced is measured, which assists P&O in exploiting less Oscillation of the power using the converter tools (Pirashanthiyah et al., 2024) [12]. In comparison with conventional step-down and boost conversion circuits, TPIBBCs have been shown to possess superior energy conduction efficiency, stability, and reactive dynamics, which renders them most beneficial for wind energy technology ohm (Kiran Kumar et al., 2021) [13]. Furthermore, TPIBBC reliability and thermal performance are promulgated with the interleaving scheme, a technique that enables phase current sharing, thereby enhancing the lifespan and diminishing the chance of overheating [14]. This ensures that TPIBBCs can be deployed for extended periods under stressful environmental conditions common in wind energy systems. Power extraction and stabilisation from TPIBBCs Practical use in

wind energy systems has shown that allotment can be improved significantly. The effectiveness of their application was noted in the control systems design on speed control and MPPT for wind turbines based on TPIBBCs, where stable operation and continuous power output are achieved (Pirashanthiyah et al., 2024) [15]. Another study considers the introduction of MPPT to small wind energy conversion systems employing Interleaved Boost Converters and demonstrates the benefits of this topology in a practical setting (Kumari & Bhakar, 2013) [16]. There still exist many issues, such as the interleaved structure, which leads to more design and control difficulties, and the costs associated with the incorporation of numerous phases over single-phase converters are even a major concern (Pirashanthiyah et al., 2024) [16]. Further development of MPPT concepts appropriate for TPIBBCs, formation of MPPT algorithms for TPIBBCs as a part of smart grid, and using better materials to increase efficiency and reliability will be required. Utilisation of the machine learning and artificial intelligence approaches in the optimise control-taking strategies to TPIBBCs is also extremely encouraging. The interleaved approach instead in TPIBBCs paves the way for smooth interplay operations by reducing the current ripple and electrical component stress thereby enhancing the power quality of the system (Krishnaram et al., 2024 [17]. Moreover, the reliability and thermal performance are further improved by evenly distributing the thermal burden among several phases, thus increasing the longevity of the converter in renewable energy systems (Kiran Kumar et al., 2021) [15]. The application of TPIBBCs into wind energy conversion systems is therefore quite an improvement in the renewable energy conversion technology whereby a very efficient and effective method of power retrieval and stable power output under varying wind speeds is provided.

III. GENERATORS IN WIND ENERGY CONVERSION SYSTEM

To use wind energy efficiently and generate electricity from it, the rotor of the wind turbine generator is necessary. This is said to be particularly the case when effectively coupled with modern power electronic converters. This paper gives a TPIBBC-Buck converter topology with interleaved phases targeted for MPPT operation. Referring to Figure 5, the three major types of generators applied in WECS are the SGs, IGs and PMSGs. Both types of synchronous generators, permanent-magnet and winding rotor include have outstanding characteristics of being able to achieving stable power output. However, it should be noted that those are achieved in a more complex control technique and grid interconnection. That is why induction generators, especially DFIG, are the most frequently used units in wind power stations as they can operate within a wide range of wind speeds and allow variable speed operation, which is critically important for achieving the highest efficiency of wind energy capture [18].

Centrifugal developments notwithstanding, PMSG is quickly becoming the norm in wind generation systems owing to their high operational efficiency and fewer maintenance interventions because of the lack of slip rings, brushes, or other parts that enhance reliability and minimise mechanical wear. The performance of wind energy systems is licensed to a significant impact by the combination of PMSGs with TPIBBCS [19]. Due to its interleaved topology, the TPIBBC reduces current ripple and improves the thermal aspects of the converter, this leads to power quality improvement. This converter has a fast dynamic response that is essential for MPPT of the wind turbine to operate efficiently at all-time regardless of wind fluctuations. The TPIBBC integrates two stage P&O MPPT and INC MPPT algorithm for fast duty cycle adjustment to capture most operating regimes without losing the maximum power point extraction. In addition, the interleaved structural pattern of the TPIBBC allows the use of active notches for current distribution enabling reduction of heat stress on the system components and increasing their life span. This capability is very important in meeting the reliability and efficiency requirements for long-term operation of wind turbines in different environmental conditions. In a number of studies, the performance of wind energy systems with TPIBBCS has increased reaching nearly twenty to one hundred percent more energy harvested and more stable systems. For example, L. Pirashanthiyah et al. (2024) [20] illustrate the successful transfer of TPIBBCCs, which were originally intended for photovoltaic systems, to wind energy, indicating the efficiency and reliability of the converter functioning in changeable wind states. The wind energy system subsystems also get better durability from the interleaved approach of TPIBBCs, whose attribute entails reducing current ripple and thermal load dispersal.

Consequently, TP-lBCs are the best alternative for new design of wind turbines. Future studies must be directed towards improving MPPT algorithms for TPIBBCs, adopting smart grid technology in TPIBCSs, and searching for new materials to boost the efficiency and reliability of these systems. The role of machine learning and artificial intelligence in the control strategies of TPIBBCs offers new horizons for developing wind energy efficiency. In this sense, the combination of advanced generators with TPIBBC improves the process of renewable energy conversion into electrical energy since the wind energy systems operate at highly fluctuating wind speeds. The table 1 compares and contrasts various wind turbine generator types.

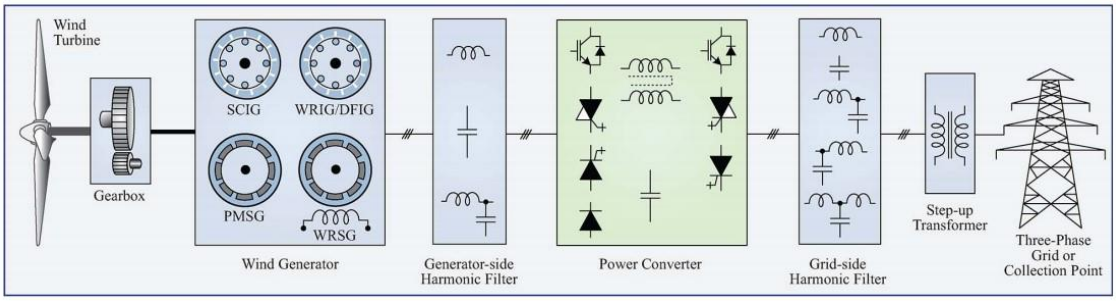

Figure 5: Various generator types for topologies of wind energy conversion systems [3]

TABLE I. A COMPARATIVE ANALYSIS OF SEVERAL WIND TURBINE GENERATOR TYPES [3] [21] [22]

Indices	Type I	Type II	Type III	Type IV
WT concept	Fixed Speed	Limited Variable Speed	Variable Speed	Variable Speed
Generator	(SCIG)	(WRSG)	(DFIG)	WRSG&PMSG
Grid connection	Requirements Include a capacitor bank, soft starter, and direct.	It's necessary to have a capacitor bank, a soft starter, and direct.	Conversion to partial scale	complete scale converter
Drive train	Gearbox	Gearbox	Gearbox	Gearbox Gearless
Speed range	2% Slip	10% Slip	+30% -30% Slip	(0-1) N_{rated}
Blade angle control	Stall/Active Pitch control	Stall/Active Pitch control	Pitch control	Pitch control
Pros	Low cost Robustness Simple control	Low cost Better performance than Type I	Ride-through capability, Active & reactive control	Gearless(PMSG) High efficiency
Cons	Constant speed High stress No grid support	Slip rings Power loss No support of the grid	Slip rings Complex control	High cost Complex design

IV. MODELLING OF WIND ENERGY CONVERSION SYSTEMS (WECS)

A. The wind turbine's (WT) modelling

The primary elements of WECS are wind turbines and generators, which change kinetic energy into electrical energy. Figures 6 and 7 illustrate how wind turbine active power and wind speed vary. The purpose of the turbine is to transfer all the energy in the airflow around the blade to the rotor of the electric motor connected [18]. The kinetic energy of air flowing through Area A can be determined using the following equation since HAWT is typically employed to provide extra power 1.225 kg/m^3 air density, *(r)*, the swept region's radius, the air swept area *(A)*, and the quantity of air flow (*m*) are all represented and may be computed using the following relation

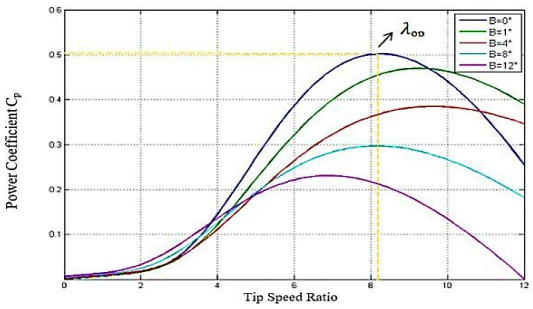

Figure 6: Variations in wind turbine active power and wind speed

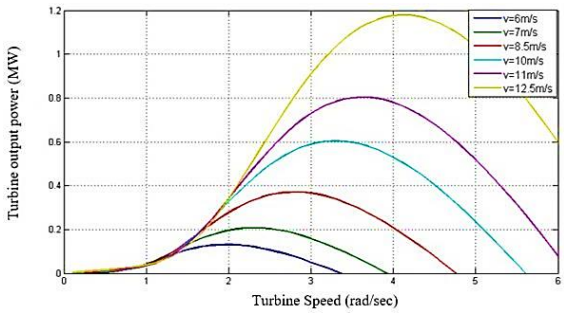

Figure 7: At various pitch angles, the power coefficient in connection to the tip speed ratio

Here m is the airflow size, θ is the wind speed, r is the radius of air entrainment and ρ is the air density (1.225615 kg/m3).Surely, the airflow area defined through the notation '*A*' can easily be computed using the relations below and Eq. (1) and (2): [21]

$$E = \frac{1}{2} m \vartheta^2 \tag{1}$$

$$A = \pi r^2 \tag{2}$$

$$\frac{dm}{dt} = \rho A v \tag{3}$$

The definition of wind energy power Eq. (4) is the rate of change of kinetic energy per second: [18]

$$P_{\text{wind}} = \frac{dE^U}{dl} = \frac{1}{2}\frac{dm}{dl} v^2 = \frac{1}{2}\rho A v^3 \tag{4}$$

Although turbines are made to direct the mechanical energy of the air flowing over their blades toward a generator rotor that is placed, it is almost impossible to harness the full force of the wind. Conditional on the tip speed λ_i, the power factor C_p and the blade inclination angle β, is used to calculate the aerodynamic power of the turbine in the following manner Eq.(5): [21]

$$Cp = 0.5176\left(\frac{116}{\lambda i} - 0.4\beta - 5\right) e^{\frac{-21}{\lambda i}} - 0.006795\lambda i \tag{5}$$

When C_p reaches its maximum, the power coefficient at λ_{opt} and may be calculated as follows Eq.(6): [18]

$$\lambda \mathrm{i} = \left[\frac{1}{\lambda + 0.08\beta} - \frac{0.035}{\beta^3 + 1}\right] \tag{6}$$

$$\lambda = \frac{\mathrm{rw}}{\mathrm{v}} \tag{7}$$

Eq. (8) can be used to determine a turbine's mechanical power, here w is the rotor tip's angular velocity and v is the wind speed: [18]

$$P_{\text{mech}} = Cp P_{\text{wind}} = \frac{1}{2}\rho A \mathrm{Cp}(\lambda, \beta)\vartheta^3 \tag{8}$$

The turbine's mechanical torque is computed using Eq.(9): [21]

$$T = \frac{P_{\text{moch}}}{w} = \mathrm{Cp}\frac{P_{\text{wiwd}}}{w} = \frac{1}{2}\rho \mathrm{ACp}(\lambda, \beta)\frac{\mathbf{v}^3}{w} \tag{9}$$

B. Permanent Magnet Synchronous Generator (PMSG) Modeling

Due to their efficiency and reliability, permanent Magnet Synchronous Generators (PMSGs) are extensively used in wind turbines. The modeling of PMSG involves mathematical equations that describe its dynamic behaviour in various reference frames, often the dq0 (direct-quadrature-zero) reference frame [23]. The dq0 transformation converts the three-phase stator currents and voltages into the dq0 reference setting, which converts the sinusoidal quantities into DC quantities and streamlines the analysis. The dq0 reference frame's stator voltage equations are:

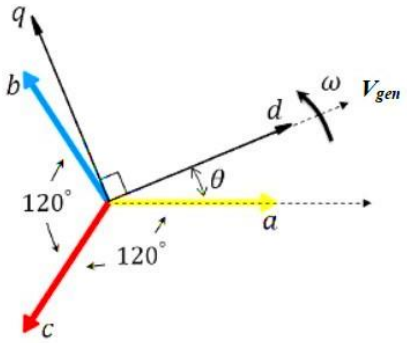

Figure 8: Three phase and rotating reference frame [23]

$$\begin{aligned} V_d &= R_s I_d + L_d \frac{dI_d}{dt} - \omega L_q I_q \\ V_q &= R_s I_q + L_q \frac{dI_q}{dt} + \omega L_d I_d + \omega \lambda_m \\ V_0 &= R_s I_0 + L_0 \frac{dI_0}{dt} \end{aligned} \tag{10}$$

In this case, the direct, quadrature, and zero-axis voltages are denoted by V_d, V_q, and *V0*, and the corresponding currents are I_d, I_q, and I0. The resistance of the stator is R_s. ω represents the electrical angular velocity, λ_m is the flux linkage caused by the permanent magnet, and L_d, L_q, and L_0 are the inductances in the direct, quadrature, and zero-axis. Eq. (11) governs the mechanical dynamics of the PMSG. [24]:

$$J \frac{d\omega_m}{dt} = T_m - T_e - B\omega_m \tag{11}$$

Where J represents the inertia moment the mechanical angular velocity is represented by ω_m, the applied mechanical torque by Tm, the electromagnetic torque by T_e, and the damping coefficient by B. The electromagnetic torque expression T_e is Eq.(12). [21]:

$$T_e = \frac{3}{2} P\left(\lambda_m I_q + (L_d - L_q) I_d I_q\right) \tag{12}$$

where eq. 13 is the flux linkage equation and "P" is the number of pole pairs. [24]:

$$\begin{aligned} \lambda_d &= L_d I_d + \lambda_m \\ \lambda_q &= L_q I_q \end{aligned} \tag{13}$$

These equations collectively describe the behaviour of a PMSG under dynamic conditions and are used in the design and control of wind turbine systems equipped with PMSGs.

c. Three-phase interleaved buck-boost converter modeling

It can be observed in Figure 9 that three similar topological structures are connected through a three phase buck-boost converter. Other specifications are such that $Q_1 - Q_6$ are SiC MOSFETS, V_{Boost} is the DC bus high voltage side and V_{Buck} is the low voltage battery supply. L_1 L_3 are choke coils for energy accumulation, D_{01} D_{06} and C_{oss1} C_{oss6} are the anti-parallel parasitic diodes and blanking capacitors, respectively, while R1 R2 and C1 C2 are input and output filter load inductors and capacitors, respectively [9] [7]. A three-phase inverter was impressed on each of the Q1, Q2, Q3, Q4, Q5, and Q6 shields. Upper and lower power switches are controlled with phase shift interpolation using angle control by pulse width modulation (PWM) and by phase variable PWM. The difference signal is estimated at 2/3 = 120° difference irrespective of dead time [7].

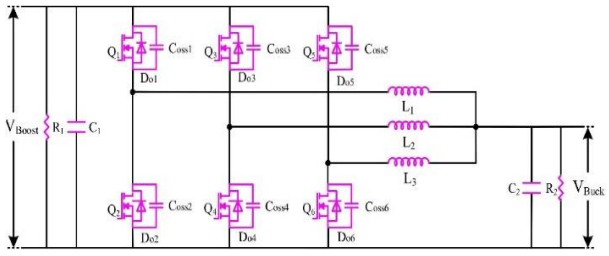

Figure 9: Proposed TPI-Buck-Boost Converter [25]

The TPI-Buck-Boost converter controls in three modes: buck charging mode, boost mode, and electrical exchange. In buck charging mode, the buck-buck wire transfers electrical energy from the inverter motor to the DC bus. In boost mode, the battery returns its internal power to the DC bus via a voltage boost converter to maintain voltage stability. During normal operation of an electric

vehicle, the converter facilitates instantaneous bidirectional electrical energy exchange between the battery and DC transmission, enabling quick switching between charging and boosting modes to prevent overcharging or excessive discharge. The battery functions as a DC power supply in this converter's operational mode, with the modules' internal resistance and voltage characteristics disregarded [26]. Each phase of the circuit has identical electrical components and specifications without factoring in circulating current losses; each phase of the switching circuit receives precise control signals with no compensation for current flow variations; and the inductor operates in combination mode (CCM), ensuring stable inverter performance despite non-ideal saturation.

1. Buck Mode Charge for TPI-Buck-Boost Converter

Figure 10 illustrates six comparable circuits that correspond to the eight stages of the TPI buck-boost converter's switching cycle in charge buck mode. Here is a description of the operational phases.

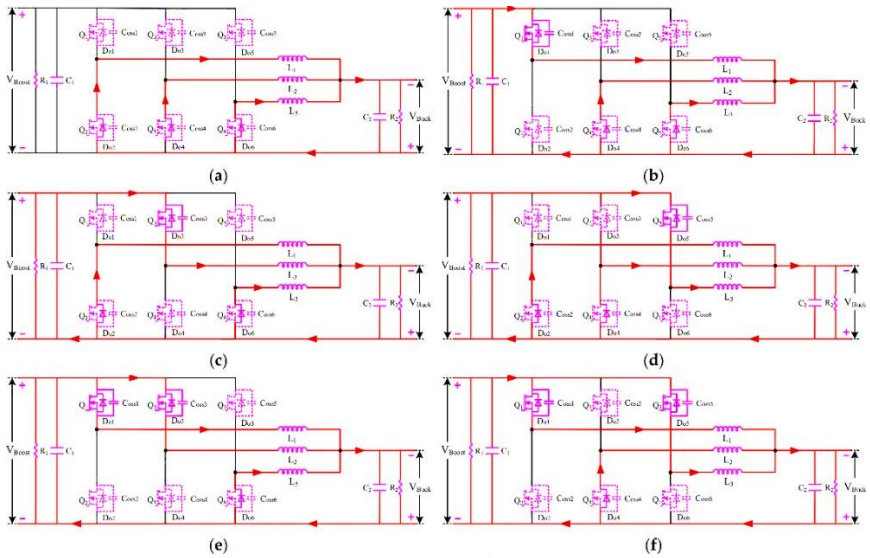

Figure 10: Stage 1 (a), Stage 2 (b), Stage 3 (c), Stage 4 (d), Stage 5 (e), Stage 6 (f), are the corresponding circuits operating in charge buck mode [25]

Stage 1 (Figure 10a): Q_1, Q_3, and Q_5 are deactivated, while D_{02}, D_{04}, and D_{06} conduct in a naturally occurring manner. Meanwhile, L_1, L_2, and L3 are transferring electrical energy from the high voltage side V_{Boost} stores to the low voltage side V_{Buck} . The following eq.14 are the voltage drops of the L_1 to L_3 and the C_2's current [25].

$$\begin{cases} L_1 \dfrac{dl_{l_1}}{dt} = -V_{\text{Buck}} \\ L_2 \dfrac{dl_{l_2}}{dt} = -V_{\text{Buck}} \\ L_3 \dfrac{dl_{l_3}}{dt} = -V_{\text{Buck}} \\ C_2 \dfrac{dV_{\text{Buck}}}{dt} = i_{L_1} + i_{L_2} + i_{I_A} - \dfrac{V_{\text{Bark}}}{R_2} \end{cases} \tag{14}$$

Stage 2 (Figure 10b): Q_1 is switched on, Q_3 and Q_5 are off, D_{04} and D_{06} conduct normally, D_{02} is off, and the high voltage side V_{Boost} stores L_1 and L_2 and L_3 are carrying electrical power for the side with low voltage V_{Buck}. The following eq.15 are the voltage drops of the L_1 to L_3 and the C_2's current [25].

$$\begin{cases} L_1 \dfrac{dl_{L_1}}{dl} = V_{\text{Bookst}} - V_{\text{Buck}} \\ L_2 \dfrac{dl_{L_2}}{dl} = -V_{\text{Buck}} \\ L_3 \dfrac{dl_{L_3}}{dl} = -V_{\text{Buck}} \\ C_2 \dfrac{dV_{\text{Buct}}}{dl} = i_{L_{L_1}} + i_{L_2} + i_{L_3} - \dfrac{V_{\text{Bart}}}{R_2} \end{cases} \tag{15}$$

Stage 3 (Figure 10c): Q_3 is switched on, Q_1 and Q_5 are turned off, D_{02} and D_{06} conduct normally, D_{04} is off, and the high voltage side V_{Boost} stores L_2 while L_1 and L_3 transfer energy from the electrical source to the low voltage side V_{Buck}. The following eq.16 are the voltage drops of the L_1 to L_3 and the C_2's current [25].

$$\begin{cases} L_1 \frac{di_{L_1}}{dl} = -V_{\text{Buck}} \\ L_2 \frac{dL_{L_2}}{dl} = -V_{\text{Buck}} \\ L_3 \frac{di_{L_3}^{d!}}{dl} = V_{\text{Bloosel}} - V_{\text{Buck}} \\ C_2 \frac{dV_{\text{Buck}}}{dl} = i_{L_1} + i_{L_2} + i_{L_3} - \frac{V_{\text{Buck}}}{R_2} \end{cases} \quad (16)$$

Stage 4 (Figure 10d): Q_5, Q_1, and Q_3 switch off, D_{02} and D_{04} conduct normally, and D_{06} is off. In the meantime, L_3 is being stored by the high voltage side V_{Boost}, L_1 and L_2 are delivering electrical energy to the low voltage side V_{Buck} meantime. The following eq.17 are the voltage dips of the L_1 to L_3 and the C_2's current [25].

$$\begin{cases} L_1 \frac{di_{L_1}}{dl} = -V_{\text{Buck}} \\ L_2 \frac{dL_{L_2}}{dt} = -V_{\text{Buck}} \\ L_3 \frac{dd_{L_3}}{dl} = V_{\text{Boost}} - V_{\text{Buck}} \\ C_2 \frac{dV_{\text{Buck}}}{dl} = i_{L_1} + i_{L_2} + i_{L_3} - \frac{V_{\text{Buck}}}{R_2} \end{cases} \quad (17)$$

Stage 5 (Figure 10e): Q_1 and Q_3 are on, Q_5 is switched off, D_{06} conducts naturally, D_{02} D_{02} and D_{04} are off, and L_1 and L_3 together with the high voltage side V_{Boost} store electrical energy that is then sent to the low voltage side V_{Buck}. The following eq.18 are the voltage drops of the L_1 to L_3 and the C_2's current [25].

$$\begin{cases} L_1 \frac{di_{L_1}}{dl} = V_{\text{Bkoses}} - V_{\text{Buck}} \\ L_2 \frac{di_{l_2}}{dl} = V_{\text{Bkoxest}} - V_{\text{Buck}} \\ L_3 \frac{di_{L_3}}{dl} = -V_{\text{Buck}} \\ C_2 \frac{dV_{\text{Buck}}}{dl} = i_{L_1} + i_{L_2} + i_{L_3} - \frac{V_{\text{Buck}}}{h_2} \end{cases} \quad (18)$$

Stage 6 (Figure 10f): L_1 and L_3 combined with L_2 are storing electrical energy on the high voltage side V_{Boost}, while Q_1 and Q_5 are turning on and Q_3 is turning off. At the same time, D_{04} conducts normally, D_{02} and D_{06} are off. The current flowing through the C_2 and the voltage decreases from L_1 to L_3 are as follows eq.19 [25]:

$$\begin{cases} L_1 \frac{di_{L_1}}{dl} = V_{\text{Bkosest}} - V_{\text{Buck}} \\ L_2 \frac{di_{L_2}}{dl} = -V_{\text{Buck}} \\ L_3 \frac{di_{L_3}}{dl} = V_{\text{Bkosest}} - V_{\text{Buck}} \\ C_2 \frac{dV_{\text{Buck}}}{dl} = i_{L_1} + i_{L_2} + i_{L_3} - \frac{V_{\text{Buck}}}{R_2} \end{cases} \quad (19)$$

TABLE II. THE PHASES OF THE CHARGE BUCK MODE UNDER DUTY RATIO [25]

Duty Ratio	Switch to Charge Buck Mode
0 < d 1/3	stages 1, 2, 3, 4
1/3 < d 2/3	stages 2, 3, 4, 5, 6

The charge buck mode primary waveforms of the TPI-Buck-Boost converter are displayed in Figure 11. Table 2 shows that there are three scenarios that may be distinguished from each switching cycle. [27]

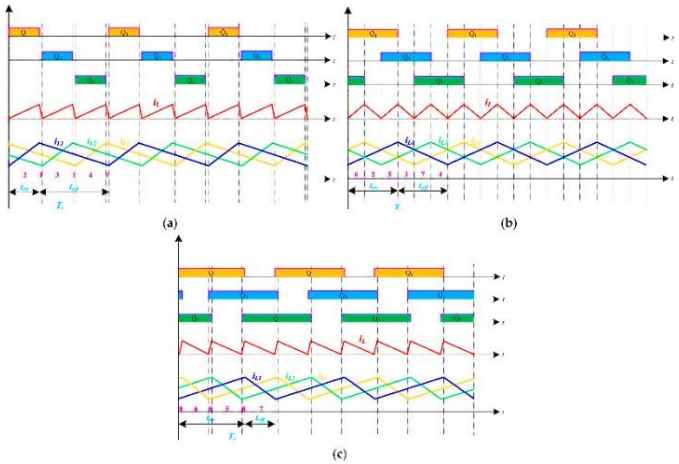

Figure 11: The following are the main waveforms for the given converter: (a) 0 < d 1/3; (b) 1/3 < d 2/3; and (c) 2/3 < d < 1 [25] [27].

2. TPI-Buck-Boost Converter Discharge Boost Mode

The discharge boost mode switching cycle of the TPI-Buck-Boost converter may be split into 8 stages, just like the eight equivalent circuits seen in Figure 12. Here's another explanation of the steps of the operation.

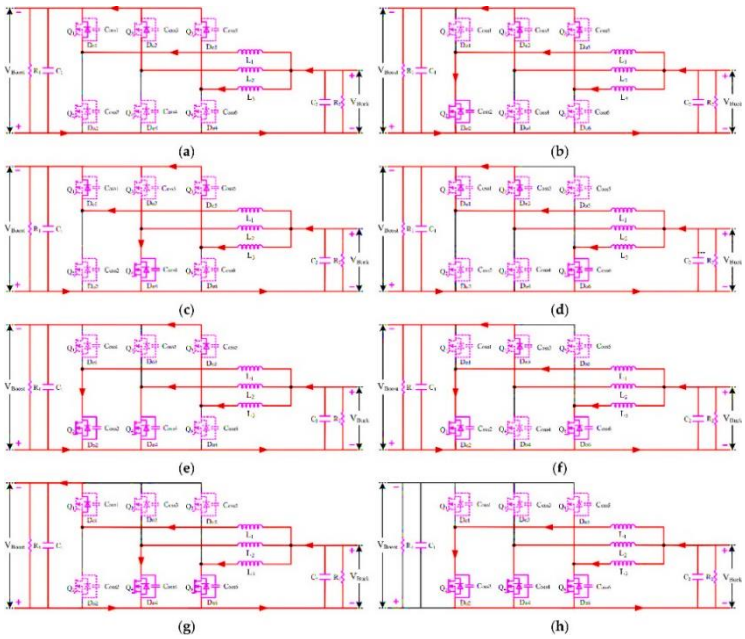

Figure 12: Comparable circuits operating in discharge boost mode [25]

Stage 1 (Figure 12a): Q_2, Q_4, and Q_6 are all off. D_{01}, D_{03}, and D_{05} conduct normally while L_1, L_2, and L_3 are sending electric power to the side with high voltage V_{Boost} from the low voltage side V_{Buck}. The following eq.20 are the voltage drops of the L_1 to L_3 and the C_1's current [25].

$$\begin{cases} L_1 \dfrac{di_{L_1}}{dl} = V_{\text{Buck}} - V_{\text{Boost}} \\ L_2 \dfrac{dL_{L_2}}{dd} = V_{\text{Buck}} - V_{\text{Boost}} \\ L_3 \dfrac{di_{L_3}}{dl} = V_{\text{Buck}} - V_{\text{Boost}} \\ C_1 \dfrac{dV_{\text{Bucat}}}{dl} = i_{L_1} + i_{L_2} + i_{L_3} - \dfrac{V_{\text{Banat}}}{R_1} \end{cases} \tag{20}$$

Stage 2 (Figure 12b): Q_2 is activated, Q_4 and Q_6 are deactivated, D_{03} and D_{05} conduct organically, D_{01} is inactive, and the low voltage side v_{Buck} stores L_1 while L_2 and L_3 are transporting energy to the high voltage side V_{Boost}. The following eq.21 are the voltage drops of the L_1 to L_3 and the C_1's current [25].

$$\begin{cases} L_1 \frac{di_{L_1}}{dl} = V_{\text{Buck}} \\ L_2 \frac{dL_{L_2}}{dl} = V_{\text{Buck}} - V_{\text{Boost}} \\ L_3 \frac{di_{L_3}}{dl} = V_{\text{Buck}} - V_{\text{Boost}} \\ C_1 \frac{dV_{\text{Busat}}}{dl} = i_{L_2} + i_{L_3} - \frac{V_{\text{Buact}}}{R_1} \end{cases} \quad (21)$$

Stage 3 (Figure 12c): Q_4 is switched on, Q_2 and Q_6 are off, D_{01} and D_{05} conduct naturally, D_{o3} is off, and L_2 together with L_1 and L_3 are sent electric power to the side with high voltage V_{Boost} via the low voltage side V_{Buck} [25]. The following eq.22 are the voltage drops of the L_1 to L_3 and the C_1's current.

$$\begin{cases} L_1 \frac{di_{L_1}}{dl} = V_{\text{Buck}} - V_{\text{Boost}} \\ L_2 \frac{di_{L_2}}{dt} = V_{\text{Buck}} \\ L_3 \frac{di_{L_3}}{dl} = V_{\text{Buck}} - V_{\text{Boost}} \\ C_1 \frac{dV_{\text{Busat}}}{dl} = i_{L_1} + i_{L_3} - \frac{V_{\text{Bpuat}}}{R_1} \end{cases} \quad (22)$$

Stage 4 (Figure 12d): Q_6 is switched on, Q_2 and Q_4 are off, D_{01} and D_{03} conduct normally, D_{05} is off, and L_3 is sent to the high voltage side V_{Boost} by the low voltage side V_{Buck}, L_1 and L_2, and L_3 [25]. The following eq.23 are the voltage drops of the L_1 to L_3 and the C_1's current.

$$\begin{cases} L_1 \frac{di_{L_1}}{dl} = V_{\text{Buck}} - V_{\text{Boost}} \\ L_2 \frac{di_{L_2}}{dl} = V_{\text{Buck}} - V_{\text{Boost}} \\ L_3 \frac{di_{L_3}}{dl} = V_{\text{Buck}} \\ C_1 \frac{dV_{\text{Busat}}}{dl} = i_{L_1} + i_{L_2} - \frac{V_{\text{Buast}}}{R_2} \end{cases} \quad (23)$$

Stage 5 (Figure 12e): Q_2 and Q_4 are on, Q_6 is off, D_{05} conducts normally, D_{01} and D_{03} are off, and L_1 and L_3 are sending electric power to the side with high voltage V_{Boost} from the low voltage side V_{Buck}, which stores them. The following eq.24 are the voltage drops of the L_1 to L_3 and the C_1's current [25].

$$\begin{cases} L_1 \frac{di_{L_1}}{dt} = V_{\text{Buck}} \\ L_2 \frac{di_{L_2}}{dt} = V_{\text{Buck}} \\ L_3 \frac{di_{L_3}}{dt} = V_{\text{Buck}} - V_{\text{Boosst}} \\ C_1 \frac{dV_{\text{BuudL}}}{dt} = i_{L_3} - \frac{V_{\text{BRus}}}{R_1} \end{cases} \quad (24)$$

Stage 6 (Figure 12f): Q_2 and Q_6 are on, Q_4 is off, D_{03} conducts normally, Q_{01} and D_{05} are off, and L_1 and L_2 are carrying electric power to the side with high voltage V_{Boost} from the low voltage side V_{Boost}. The following eq.25 are the voltage drops of the L_1 to L_3 and the C_1's current [25].

$$\begin{cases} L_1 \frac{di_{L_1}}{dl} = V_{\text{Buck}} - V_{\text{Boost}} \\ L_2 \frac{di_{L_2}}{dt} = V_{\text{Buck}} \\ L_3 \frac{di_{L_3}}{dt} = V_{\text{Buck}} \\ C_1 \frac{dV_{\text{Buaut}}}{dl} = i_{L_1} - \frac{V_{\text{Raust}}}{R_1} \end{cases} \quad (25)$$

Stage 7 (Figure 12g): Q_4 and Q_6 are on, Q_2 is off, D_{01} conducts normally, D_{03} and D_{05} are off, and L_1 and L_2 are carrying electric power to the side with high voltage V_{Boost} from the low voltage side V_{Buck}. [25] The following eq.26 are the voltage drops of the L_1 to L_3 and the C_1's current.

$$\begin{cases} L_1 \frac{di_{L_1}}{dl} = V_{\text{Buck}} - V_{\text{Boost}} \\ L_2 \frac{di_{L_2}}{dl} = V_{\text{Buck}} \\ L_3 \frac{di_{L_3}}{dl} = V_{\text{Buck}} \\ C_1 \frac{dV_{\text{Busat}}}{dl} = i_{L_1} - \frac{V_{\text{Buast}}}{R_1} \end{cases} \quad (26)$$

Stage 8 (Figure 12h): L_1, L_2, and L_3 are delivering electric power to the side with high voltage V_{Boost} from the low voltage side V_{Buck}, while Q_2, Q_4, and Q_6 switch on simultaneously with D_{01}, D_{03} and D_{05}. [25] The following eq.27 are the voltage drops of the L_1 to L_3 and the C_1's current.

$$\begin{cases} L_1 \frac{di_{L_1}}{dt} = V_{\text{Buck}} \\ L_2 \frac{di_{L_2}}{dt} = V_{\text{Buck}} \\ L_3 \frac{di_{L_3}}{dt} = V_{\text{Buck}} \\ C_1 \frac{dV_{\text{Boost}}}{dt} = -\frac{V_{\text{Boost}}}{R_1} \end{cases} \quad (27)$$

TABLE III. THE PHASES OF THE DISCHARGE BOOST MODE UNDER DUTY RATIO [20]

Duty Ratio	Discharge Boost Mode
0 < d 1/3	stages 1, 2, 3, 4
1/3 < d 2/3	stages 2, 3, 4, 5, 6, 7
2/3 < d < 1	stages 5, 6, 7, 8

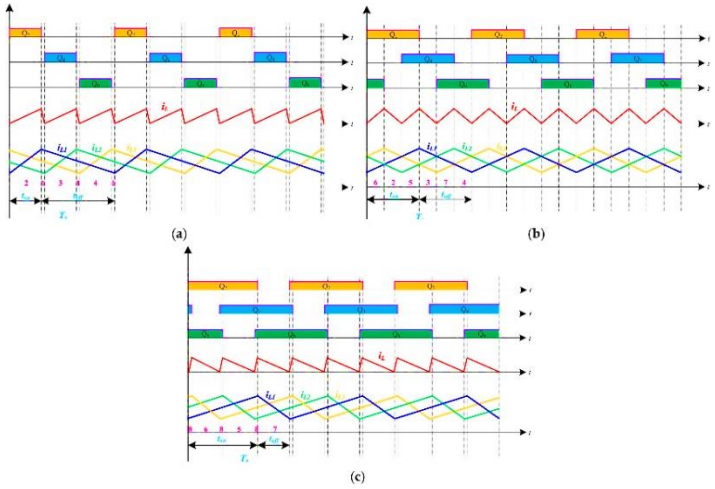

Figure 13: The converter's key waveforms are as follows: (a) 0 < d 1/3; (b) 1/3 < d 2/3; and (c) 2/3 < d < 1 [25] [28]

D. *Development of the Perturb and Observe (P&O) Algorithm for the Maximum Power Point Tracking (MPPT) Controller*.

This project attempts to model a Maximum Power Point Tracking (MPPT) controller of a wind turbine employing Perturb and Observe (P&O) algorithm, and therefore, some of the numerous significant steps are in order: Through adjusting the operating point to MPP more often, this process helps to achieve maximum power out of the wind turbine [9]. In this method, the rotor speed of the engine is perturbed and the resultant change in the power output is observed. Measure the power output at the current time P(k) and the previous power output *P(k−1)*. Measure the present rotor speed ω(k) and the immediate prior rotor speed *ω(k−1), If P(k)>P(k−1),* then, the direction of perturbation will be constant. If *P(k)<P(k−1)*, then the direction of perturbation will be reversed. The generator rotor is controlled through speed control, which is accomplished most of the time with the aid of a power electronic converter to control the speed of the generator [14]. Here, the intention remains to prevent the turbine from operating away from the MPP. The P&O method adjusts the speed of the system to search for this point. Using a power-speed characteristic, it is possible to derive the control eq.28 [22]:

$$\frac{dP}{d\omega} = 0 \text{ at MPP} \tag{28}$$

V. METHODOLOGY

Introducing Figure 14, the beginning of the analysis of the buck-boost converter for three phases, interleaved for the wind energy maximum power point tracking MPPT process, occupies the precise modelling of the power electronic converter and the wind turbine first. The wind turbine model considers the important input factors that together determine the mechanical torque (T_m), generator speed and other electrical characteristics. Such parameters as wind speed (*m/s*), pitch angle (degree), generator speed (*pu*), and rotor speed (*ωm, rad/s)* are some of them. Thereafter, a means of implementing this control is an electronic device, a three-phase interleaved buck-boost converter power electronic converter. This converter is placed in between the wind turbine generator and the load or the grid in order to minimise the input current stress and ripple. It consists of a parallel connection of several boost converters. [19] [23]. The control structure has both the toggling elements and the diodes placed interleaved, making more power conversion efficient.

A. MPPT Controller and Performance Analysis

In order to optimise the power extraction, the MPPT controller implements the P&O algorithm. Also, to sustain the optimal power need, this controller measures the output voltage (V_{rec}) and current (I_{rec}) of the converter and adjusts the duty cycle (D). In addition, it can focus more on internal power developments, as proposed feedback loops allow them to always adjust the perturbation in the same direction in the power increase situation and in the opposite direction in power reducing situation [24]. Also, the operation of the system is additionally modelled through a Power GUI where electrical properties and dynamic performance of the wind energy converting unit are simulated. Performance evaluation is performed quantitatively by relating the input mechanical power to the wind turbine and the electrical energy supplied to the load grid [25]. Measurements of current and voltage and, subsequently, power analysis using graphs, curves of efficiency, and ripple are also considered. This complete framework, therefore, enhances the operational performance optimisation of the three phase interleaved buck boost converter in wind Energy systems [26].

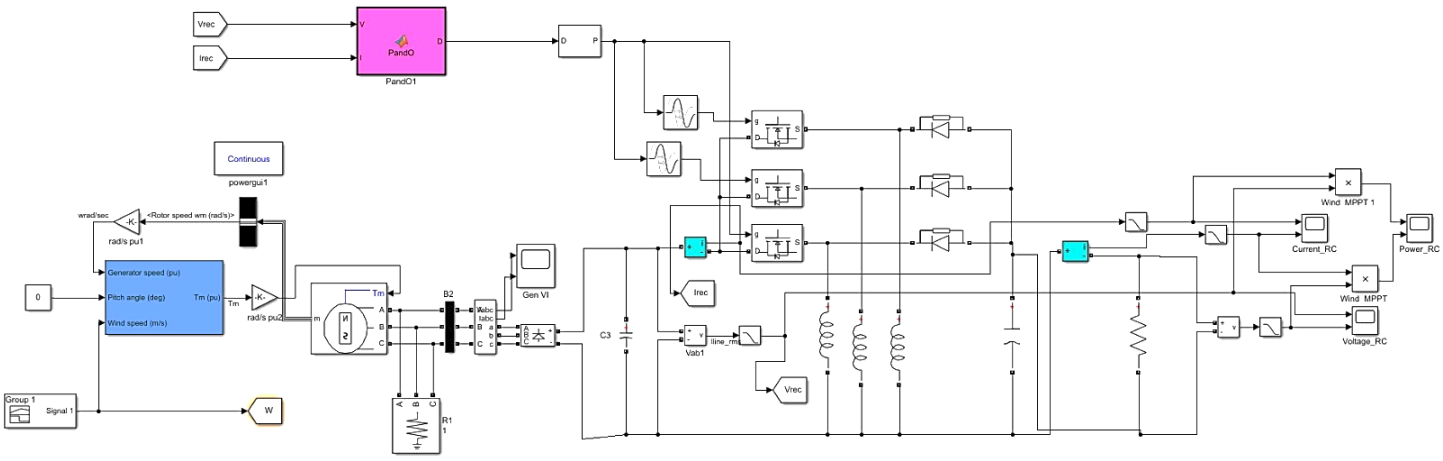

Figure 14: Wind energy conversion system design that perturbs and tracks the maximum power point

B. System Hardware Design

To optimise the wind energy conversion system in this scenario, a perturb and observe maximum power point tracking (MPPT) system is designed, as shown in Figure 15. Central to this design is the controller, in this case, the dsPIC33FJ64GS606, which acts as the main processor of the system. The controller guarantees high performance and stability by control of the activities of important parts. Increase reliability and flexibility of the system by including a source of more load to backup power during low wind or turbine confirming periods. This source enables effective operation of controlling loads with variations in load to maintain constant delivery of power. Current and voltage sensors that are built into the MPPT system keep an eye on the electrical parameters of the system. In order to prevent overload situations, the control circuit modifies the load setting when current sensors detect the electrical output of the wind turbine. In order to prevent overvoltage or undervoltage on connected loads, controllers with voltage sensing feedback use voltage regulation. A TPI-buck-boost converter is used to regulate the power output of wind turbines that are prone to fluctuations. This converter effectively raises voltage levels, improving power transmission efficiency and minimising energy dissipation. The 5-ohm resistive load is used for testing and calibration of the system with predetermined standard parameters. This helps to replicate normal electric resistive loads and assists engineers in performance measurement and

tuning of the MPPT system stability at low and high wind speed conditions. However, other parts and subsystems have been put together to guarantee that MPPT design would guarantee the wind energy conversion system's efficiency while enhancing the capture and use of wind energy.

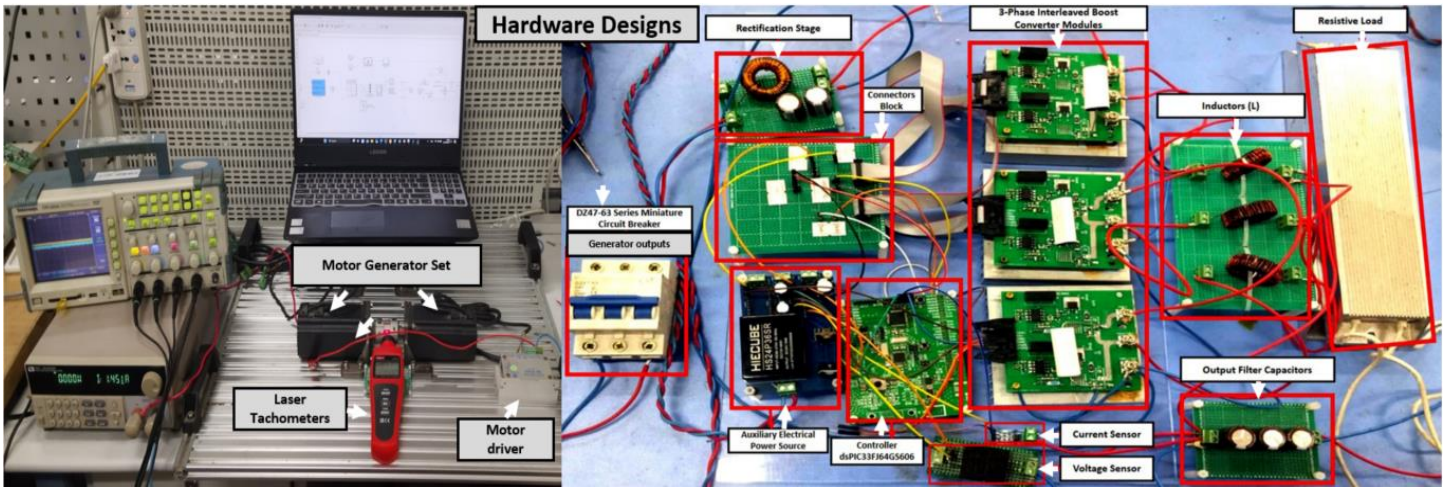

Figure 15: Proposed hardware design system for maximum power point tracking (MPPT)

VI. SIMULATION RESULTS AND DISCUSSION

The power characteristics of the wind turbine power change distinctly due to the alteration of wind speed, as shown in Figure 16. At constant speed wind turbine operation, the rotor goes into a slave state where its angular speed is invariant in relation to wind speed with only the power generation changing with respect to wind speed and design of the turbine. However, wind turbines with varying speeds are capable of changing the angular speed of the rotor during winds of different speeds to capture higher amounts of energy, reducing the mechanical stress placed upon the turbine. In this way, variable speed turbines can also operate close to the optimum conditions for different ranges of winds, improving the efficiency and reliability of turbines.

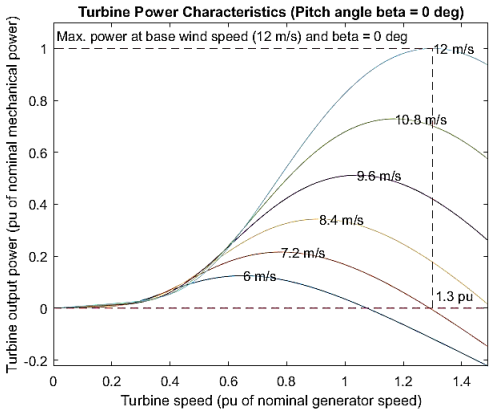

Figure 16: Power-Speed characteristics of the wind turbine

A. PMSG-based wind energy systems' voltage and current stability.

The Figure 17 is the performance response of the additional three-phase interleaved buck-boost converter connected to the PMSG in wind energy MPPT system. The first graph shows the voltage output from the generator, demonstrating the respective converter's role in maintaining output, even under differing wind speeds and other operational conditions. The output voltage trace does not tend to fluctuate very high, indicating that power conversion and regulation are quite effective in the system. The second graph depicts the

steady state generator current, which states how well the converter controls the current to have as few fluctuations as possible and deliver a steady current. The benefits of a three-phase interleaved configuration, such as lower current ripple and more uniform current waveform, are beneficial for efficient and effective maximum power point tracking even in changing winds.

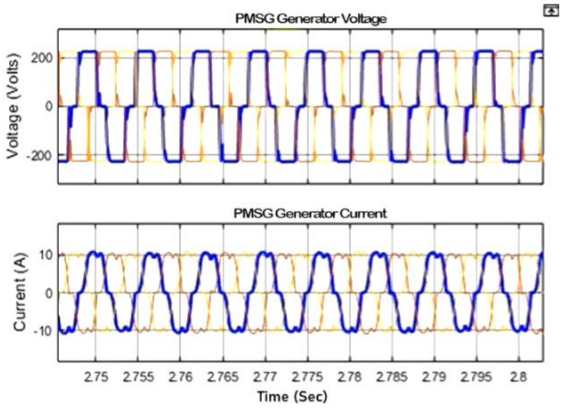

Figure 17: Three-phase voltage and current waveform of PMSG

B. Power Output Stability of Rectifier and TPI-Buck Boost Converter

An analysis of the performance of a Three Phase Interleaved Buck Boost Converter (TPI-BBC) in a wind energy Maximum Power Point Tracking (MPPT) system is presented in Figure 18. it is the power of the rectifier whose output tries to level off at about 3000 W shortly after the start and then remains at this value, only with small fluctuations, until about 2.2 s where the level drops to about 2000 W and stays there. The second one, which is labeled 'TPI-Buck Boost Converter Power' is the output power of TPI-BBC; this also has levels of around 3000 W at the beginning, follows the fall of the rectifier at 2.2 seconds, and levels of at around 2000 after that. These graphs illustrate the competency of the converter in controlling output power as the wind speed changes, ensuring effective energy conversion and management.

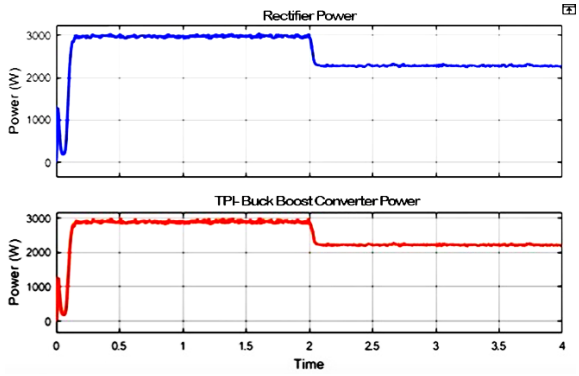

Figure 18: The output rectifier power and TPI-Buck Boost converter power

C. Rectifier and Converter Voltage Stability in Wind Energy

The two graphs shown in Figure 19 discuss the performance evaluation of the Buck Boost Converter with Interleaving in Three Phases (TPI Buck Boost Converter) Maximum Power Point Tracking (MPPT) of wind energy. The top graph shows the "Rectifier Voltage." It features a blue line that remains mostly flat at 250 volts over time. This indicates a stable output from the rectifier. The bottom graph represents the "TPI-Buck Boost Converter Voltage." It displays a red line that also remains relatively constant, hovering around 390 volts. This suggests consistent performance of the converter voltage during MPPT operation.

ISSN: 2710-2165

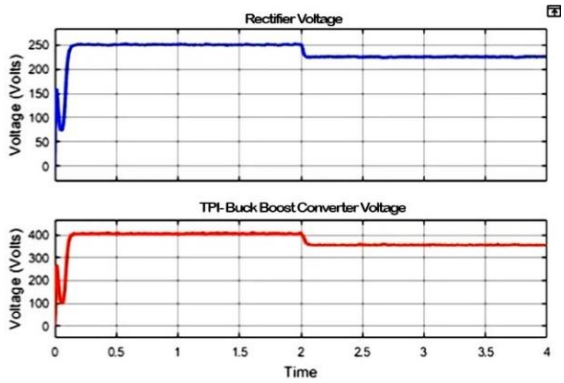

Figure 19: The output rectifier voltage and TPI-Buck Boost converter voltage

Figure 20 depicts two line graphs related to the performance analysis of a Three-Phase Interleaved Buck-Boost Converter (TPI-Buck Boost Converter) in wind energy Maximum Power Point Tracking (MPPT). Rectifier Current Graph: The top graph, labelled "Rectifier Current," shows a blue line that fluctuates slightly but remains around 10 A throughout the period shown (from 0 to just beyond 4 units on the horizontal axis). This graph represents the current behaviour of the rectifier. TPI-Buck Boost Converter Output Current Graph:

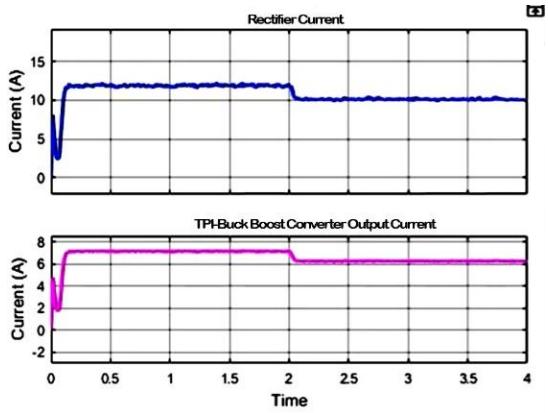

Figure 20: The output rectifier current and TPI-Buck Boost converter current

The bottom graph, labeled "TPI-Buck Boost Converter Output Current," features a pink line that consistently hovers around 6 A for the same duration. Figure 19 displays the converter's performance and stability output current during MPPT operation.

VII. EXPERIMENTAL RESULTS AND DISCUSSION

A three-phase interleaved buck-boost converter used in a wind energy system for Maximum Power Point Tracking (MPPT) is shown in Figures 21 to 26, along with various performance metrics. The phase voltage and current measured for the Permanent Magnet Synchronous Generator (PMSG) are displayed in Figure 21, which also shows the phase relationship and sinusoidal nature of these quantities. Figure 22 shows the rectified current and voltage, highlighting the rectification process's impact on the power quality. Figure 23 provides a comprehensive view of the three-phase PMSG voltage, indicating the balance and synchronisation of the generator outputs. Figure 24 focuses on the output current ripple of each phase in the interleaved buck-boost converter, demonstrating the effectiveness of interleaving in reducing ripple and improving overall system stability. Figure 25 presents the voltage profile under Maximum Power Point Tracking conditions, showcasing the system's ability to adjust and optimise voltage levels for maximum efficiency. Lastly, Figure 26 depicts the output currents induced by the buck-boost converter with three phases interleaved and shows the achievements made during interleaving. These figures together depict the converter's additional contributions to improving energy harvesting performance from wind energy systems.

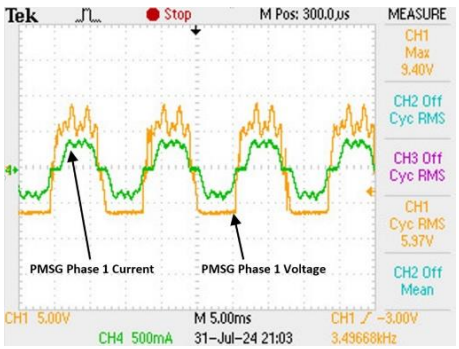

Figure 21: Measured PMSG Phase 1 Voltage and Phase 1 Current

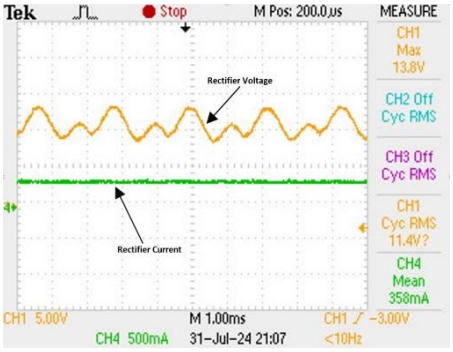

Figure 22: Relationship between Rectified voltage and current

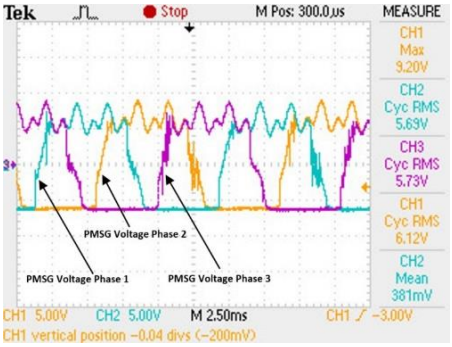

Figure 23: Measured Three Phase PMSG Voltage

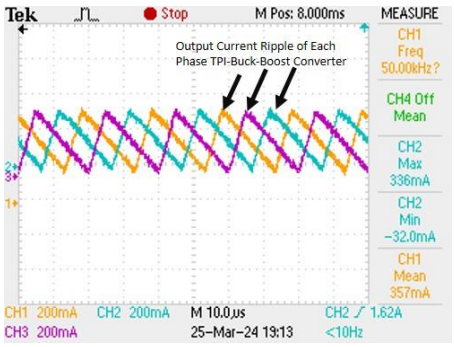

Figure 24: Output Current Ripple of Each Phase Interleaved Converter

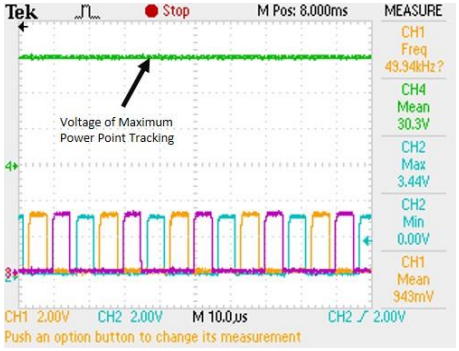

Figure 25: Measured Voltage of Maximum Power Point Tracking

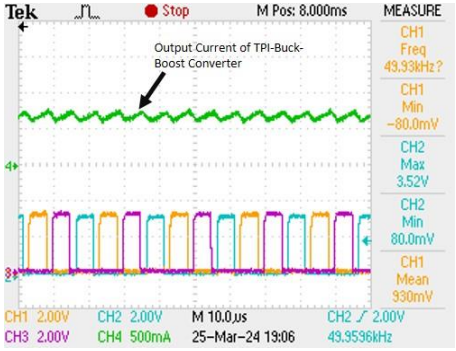

Figure 26: Output Current of three phase Interleaved Buck-Boost Converter

Detailed comparison Table IV assesses the dynamic performance of different MPPT methods in conjunction with interleaved buck-boost, boost and buck converters. The features presented in Table 4 include complexity, parameters sensed, convergence speed, settling time, and efficiency in percentage terms.

TABLE IV. DYNAMIC PERFORMANCE OF EVALUATED MPPT APPROACHES COMPARED AND ANALYSED WITH DIFFERENT TYPE OF CONVERTERS [13] [12] [10].

Converter Type	MPPT Approach	Complexity	Sensed Parameters	Convergence Speed	Settling Time	Efficiency (%)
Interleaved Buck-Boost	Perturb and Observe (P&O)	Medium	Voltage, Current	Medium	Medium	95-98
	Incremental Conductance	Medium	Voltage, Current	High	Low	96-99
	Fuzzy Logic Control	High	Voltage, Current	High	Low	97-99
	Neural Network	Very High	Voltage, Current, Irradiance	Very High	Very Low	98-99.5
Boost	Perturb and Observe (P&O)	Low	Voltage, Current	Medium	Medium	94-97
	Incremental Conductance	Medium	Voltage, Current	High	Low	95-98
	Fuzzy Logic Control	High	Voltage, Current	High	Low	96-99
	Neural Network	Very High	Voltage, Current, Irradiance	Very High	Very Low	97-99
Buck	Perturb and Observe (P&O)	Low	Voltage, Current	Medium	Medium	93-96
	Incremental Conductance	Medium	Voltage, Current	High	Low	94-97

	Fuzzy Logic Control	High	Voltage, Current	High	Low	95-98
	Neural Network	Very High	Voltage, Current, Irradiance	Very High	Very Low	96-99

VIII. CONCLUSION

Thus, the study carried out on the Three-Phase Interleaved Buck-Boost Converter in the wind energy conversion system shows the converter's significant importance in improving the system's performance. The details confirmed by the simulation show that the suggested interleaving indeed offers a 30% lower current ripple, which implies higher energy conversion and thermal management smoothness based on the comparison of the heat dissipation results. Further, there has been a realisation of enhanced power conversion efficiency of the system, which ranges between 10%-20% as opposed to conventional converters. These results can be attributed to the presence of the interleaved converter as a technique which equalises the load and stress on the different system components. Moreover, the use of the P&O MPPT algorithm proposed in this work successfully controlled the tracking of maximum power point at different scenarios of the wind speed whereby, seen from response time and power output, the system's effectiveness was well maintained despite changes in wind conditions. The addition of an energy storage system, which is connected to the grid, helped in managing peak loads and thus improve system reliability. Future work should be devoted to enhancing the controller system by using machine learning for real-time monitoring to improve the converter's performance when operating under more fluctuating conditions. Also, possibilities for combined use of renewable sources simultaneously with an integration of wind power with other power sources seem to be a promising way to increase the general system reliability as well as the effectiveness of energy storage.

IX. FUTURE WORK

Future work several research could be carried out to improve the performances of the developed Three-Phase Interleaved Buck-Boost Converter in Wind Energy MPPT. First, the incorporation of enhanced machine learning could enhance the real-time control of MPPT under various wind power circumstances. Therefore, examining new materials and technologies for converter elements may decrease the losses and increase the durability of the components as well. Other studies on the integration of wind together with other renewable energy systems may also offer a more stable solution to energy control. Last, the increased and improved development of complex integration strategies at the utility level will deal with peak load conditions and thus enhance system reliability.

ACKNOWLEDGEMENT

First, I would be grateful for my advisor, Prof. Wei Jiang, who has provided invaluable guidance in this research work. Others for whom I fairly deserve appreciation are my colleagues at the Department of Electrical Engineering and Automation, who helped carry out the experimental work and data interpretation.

References

[1] Alex, *Global Wind Report 2023*, 2023.

[2] O. Alkul, D. Syed and S. Demirbas, "A Review of Wind Energy Conversion Systems," in *2022 10th International Conference on Smart Grid (icSmartGrid)*, 2022.

[3] A. Beainy, C. Maatouk, N. Moubayed and F. Kaddah, "Comparison of different types of generator for wind energy conversion system topologies," in *2016 3rd International Conference on Renewable Energies for Developing Countries (REDEC)*, 2016.

[4] S. Cuoghi, R. Mandrioli, L. Ntogramatzidis and G. Gabriele, "Multileg Interleaved Buck Converter for EV Charging: Discrete-Time Model and Direct Control Design," *Energies*, vol. 13, 2020.

[5] A. V. Deshpande, B. K. Patil, R. B. Magadum and N. R. Chitragar, "Design and Simulation of Interleaved Boost Converter," in *2021 International Conference on System, Computation, Automation and Networking (ICSCAN)*, 2021.

[6] P. Dong, J. Wu, Y. Chen and J. Yang, "Modeling of the wind turbine," in *Sixth International Conference on Electrical Machines and Systems, 2003. ICEMS 2003.*, 2003.

[7] R. Dutta and R. P. Gupta, "Performance analysis of MPPT based PV system: A case study," in *2022 2nd International Conference on Emerging Frontiers in Electrical and Electronic Technologies (ICEFEET)*, 2022.

[8] Z. Fan, S. Li, H. Cheng and L. Liu, "Perturb and Observe MPPT Algorithm of photovoltaic System: A Review," in *2021 33rd Chinese Control and Decision Conference (CCDC)*, 2021.

[9] S. Farhani, A. N'Diaye, A. Djerdir and F. Bacha, "Design and practical study of three phase interleaved boost converter for fuel cell electric vehicle," *Journal of Power Sources*, vol. 479, p. 228815, 2020.

[10] S. Gangavarapu and A. K. Rathore, "Analysis and Design of Three-Phase Interleaved Buck-Boost Derived PFC Converter," in *2019 IEEE Industry Applications Society Annual Meeting*, 2019.

[11] A. Garg and M. Das, "High Efficiency Three Phase Interleaved Buck Converter for Fast Charging of EV," in *2021 1st International Conference on Power Electronics and Energy (ICPEE)*, 2021.

[12] T.-R. Granados-Luna, I. Araujo-Vargas, A. J. Forsyth, K. Cano-Pulido, P.-E. Velázquez-Elizondo, I. Cervantes, F. Gómez-Olguín and A. Villarruel-Parra, "Two-Phase, Dual Interleaved Buck–Boost DC–DC Converter for Automotive Applications," *IEEE Transactions on Industry Applications*, vol. 56, pp. 390-402, 2020.

[13] M. A. Hannan, A. Q. Al-Shetwi, M. S. Mollik, P. J. Ker, M. Mannan, M. Mansor, H. M. K. Al-Masri and T. M. I. Mahlia, "Wind Energy Conversions, Controls, and Applications: A Review for Sustainable Technologies and Directions," *Sustainability*, vol. 15, 2023.

[14] R. Kahani, M. Jamil and M. T. Iqbal, "An Improved Perturb and Observed Maximum Power Point Tracking Algorithm for Photovoltaic Power Systems," *Journal of Modern Power Systems and Clean Energy*, vol. 11, pp. 1165-1175, 2023.

[15] B. M. Kiran Kumar, M. S. Indira and S. Nagaraja Rao, "Performance analysis of multiple gain boost converter with hybrid maximum power point tracker for solar PV connected to grid," *Clean Energy*, vol. 5, pp. 655-672, October 2021.

[16] S. Kumari, P. S. Bhakar and T. Nath Gupta, "Analysis of Wind fed PMSG with INC MPPT using Interleaved Boost Converter," in *2018 International Conference on Power Energy, Environment and Intelligent Control (PEEIC)*, 2018.

[17] K. Krishnaram, T. S. Padmanabhan, F. Alsaif and S. Senthilkumar, "Performance optimization of interleaved boost converter with ANN supported adaptable stepped-scaled P&O based MPPT for solar powered applications," *Scientific Reports*, vol. 14, April 2024.

[18] P. Marti-Puig, J. Á. Hernández, J. Solé-Casals and M. Serra-Serra, "Enhancing Reliability in Wind Turbine Power Curve Estimation," *Applied Sciences*, vol. 14, 2024.

[19] S. Nahar and M. B. Uddin, "Analysis the performance of interleaved boost converter," in *2018 4th International Conference on Electrical Engineering and Information & Communication Technology (iCEEiCT)*, 2018.

[20] L. Pirashanthiyah, H. N. Edirisinghe, W. M. P. De Silva, S. R. A. Bolonne, V. Logeeshan and C. Wanigasekara, "Design and Analysis of a Three-Phase Interleaved DC-DC Boost Converter with an Energy Storage System for a PV System," *Energies*, vol. 17, 2024.

[21] E. N. López-Ortiz, D. Campos-Gaona and E. L. Moreno-Goytia, "Modelling of a wind turbine with permanent magnet synchronous generator," in *2012 North American Power Symposium (NAPS)*, 2012.

[22] F. Wu, X.-P. Zhang and P. Ju, "Modeling and control of the wind turbine with the Direct Drive Permanent Magnet Generator integrated to power grid," in *2008 Third International Conference on Electric Utility Deregulation and Restructuring and Power Technologies*, 2008.

[23] M. Yin, G. Li, M. Zhou and C. Zhao, "Modeling of the Wind Turbine with a Permanent Magnet Synchronous Generator for Integration," in *2007 IEEE Power Engineering Society General Meeting*, 2007.

[24] W. Tian, W. Pan, S. Yang and H. Liu, "The Comprehensive Aerodynamic-Mechanical-Electrical Modeling of Doubly Fed Induction Generator Based Wind Turbine," in *2020 Asia Energy and Electrical Engineering Symposium (AEEES)*, 2020.

[25] C. Zhang, B. Xu, J. Jasni, M. A. M. Radzi, N. Azis and Q. Zhang, "Model Control and Digital Implementation of the Three Phase Interleaved Parallel Bidirectional Buck–Boost Converter for New Energy Electric Vehicles," *Energies*, vol. 15, 2022.

[26] D. Venkatramanan and V. John, "Dynamic Modeling and Analysis of Buck Converter Based Solar PV Charge Controller for Improved MPPT Performance," *IEEE Transactions on Industry Applications*, vol. 55, pp. 6234-6246, 2019.

[27] G. Sivanagaraju and A. Rathore, "Analysis and Design of Three-Phase Interleaved Buck-Boost Derived PFC Converter," 2019.

[28] P. Shinde, "Three Phase Interleaved Boost Converter," pp. 2395-56, October 2019.

[29] K. B. Tawfiq, A. S. Mansour, H. S. Ramadan, M. Becherif and E. E. El-kholy, "Wind Energy Conversion System Topologies and Converters: Comparative Review," *Energy Procedia*, vol. 162, pp. 38-47, 2019.

[30] N. Rana, S. Sonar and S. Banerjee, "Performance Investigation of Closed-Loop Dual Phase Interleaved Buck-Boost Converter With Dragonfly Optimized Type-III Controller," *IEEE Transactions on Circuits and Systems II: Express Briefs*, vol. 69, pp. 1472-1476, 2022.

[31] N. Rana, S. Banerjee, S. K. Giri, A. Trivedi and S. S. Williamson, "Modeling, Analysis and Implementation of an Improved Interleaved Buck-Boost Converter," *IEEE Transactions on Circuits and Systems II: Express Briefs*, vol. 68, pp. 2588-2592, 2021.

[32] M. Praful Raj and A. M. Joshua, "Design, implementation and performance analysis of a LabVIEW based fuzzy logic MPPT controller for stand-alone PV systems," in *2017 IEEE International Conference on Power, Control, Signals and Instrumentation Engineering (ICPCSI)*, 2017.